Dhaka Univ. J. Sci. 74(1): 62-68, 2026 (January)
Prof. M. Muhibur Rahman Memorial Issue
ISSN 1022 - 2502, E-ISSN 2408- 8528
DOI: https://doi.org/10.3329/dujs.v74i1.84622

Modeling and Simulation of a Nanofluid-Cooled Microchannel Sawtooth Cooling Device

Shugata Ahmed[1*] and Muhammad Hasibul Hasan[2]

[1]*Departmental of Robotics and Mechatronics Engineering, Faculty of Engineering and Technology, University of Dhaka, Dhaka 1000, Bangladesh*
[2]*Departmental of Mechanical and Industrial Engineering, Faculty of Engineering and Architectural Science Ryerson University, Canada*

(Received : 25 September 2025 ; Accepted : 1 January 2026)

Abstract

The purpose of this paper is to numerically investigate the heat transfer and pressure drop characteristics of a microchannel sawtooth cooling device for Al_2O_3-water, CuO-water, and TiO_2-water nanofluid coolants. Results are compared with rectangular single-layer microchannel heat sinks (SL-MCHS) and double-layer microchannel heat sinks (DL-MCHS) of the same geometrical features. Numerical simulation has been carried out by the commercial software FLUENT 14.5 release. Governing equations are solved by the finite volume method. The pressure-velocity coupling equation is solved using the Semi-Implicit Method for Pressure Linked Equations (SIMPLE) algorithm. The thermal resistance of the microchannel sawtooth cooling device is lower than SL-MCHS and DL-MCHS. Thermal resistance of the heat sink is influenced by the volume fraction of nanoparticles, geometrical parameters, and pumping power.

Keywords: microchannel sawtooth cooling device, microchannel heat sink, nanofluids

I. Introduction

Thermal control of microelectronic devices and MEMS is one of the requirements for their reliability. Therefore, microscale heat transfer from tiny electrical and electromechanical devices is a cutting-edge research area.

Tuckerman and Peace[1] created microchannel heat sinks to dissipate large amount heat encrgy integrated circuits. Dickey and Lam[2] introduced a sawtooth cooling system that consists of alternating isosceles triangular microchannels. Fluid flow and heat transfer were simulated in a variety of microchannels by Gunnasegaran et al.[3]. They discovered that triangular microchannel heat sinks exhibit inferior performance when contrasted with rectangular and trapezoidal ones. Nevertheless, Asgari and Saidi[4] have determined that triangular microchannels exhibit a higher dimensionless heat transfer rate than other geometries. Xia et al.[5] accelerated fluid mixing and perturbed the boundary layer in microchannels to enhance heat transfer by incorporating triangular cavities. Kim et al.[6] developed an analytical model to determine heat transfer rates for rectangular, trapezoidal, triangular, and diamond channels by analyzing fin efficacy.

Microchannel heat sinks contain a minimal liquid refrigerant. The minimal quantity of fluid is incapable of withstanding elevated surface temperatures. This results in an increase in the temperature of the fluid in the direction of flow. Consequently, the surface temperature increases in a streamwise manner as the fluid-surface temperature differential decreases. For this reason, Vafai and Zhu[7] developed the double-layered microchannel heat sink (DL-MCHS) to enhance the flow of fluid in the upper layer, thereby facilitating uniform surface heating. Hazli et al.[8] and Seder et al.[9] conducted research on triangular double-layer microchannels. Hung and Yan[10] compared DL-MCHS to a single-layer channel. They discovered that the temperature difference between the fluid surface and the exit region of the DL-MCHS falls, while the temperature difference between the countercurrent flow and the exit region of the SL-MCHS increases. In double-layer microchannels, Wong and Muezzin[11] investigated the transmission of heat in parallel and counterflow mode. Chong et al.[12] and Shao et al.[13] optimized DL-MCHS to decrease heat resistance and pumping power. To enhance thermal performance, Hung et al.[14] enhanced the geometrical parameters of DL-MCHS.

In this paper, a microchannel sawtooth cooling device is compared to a DL-MCHS by simulation. A complete mathematical model is provided. Aluminum is considered as the channel material. As coolants, Al_2O_3-water, CuO-water, and TiO_2-water nanofluids are considered. Nanoparticle volume fraction, channel width and height ratio, and pumping power are considered variables, while the size of nanoparticles is fixed at 0.02 mm. The total thermal resistance of the heat sink has been calculated.

II. Materials and Methods

Physical description

In Fig. 1, three-dimensional views of the microchannel sawtooth cooling device and the rectangular double-layer microchannel heat sink are shown. However, for comparison purposes, it is necessary to consider equal cross-sections of both of the channels. For this reason, four rectangular double-layer microchannels are considered in the simulation (Fig. 1). The fin width, W_f is double the gap between upper and lower channels (Fig. 1a). Two single-layer channels are formed by joining one upper and lower channel of height H_{ch_up} and H_{ch_low} respectively (Fig. 1b).

*Author for correspondence. e-mail: shugataahmed.rme@du.ac.bd

Again, a half-triangular and half-inverted-triangular shape is formed by intersecting one single-layer channel diagonally (Fig. 1c). Then two half-triangular channels are joined to form one complete triangular channel with two half-inverted triangular channels on both sides of height H_{ch} (Fig. 1d). By this transformation, it is verified that the considered heat sinks, DL-MCHS, SL-MCHS, and microchannel sawtooth devices, have the same cross-sectional area although the surface area is different. Hence, it can be predicted that differences in heat transfer characteristics of these heat sinks originate from their variable surface area while operated under the same boundary conditions.

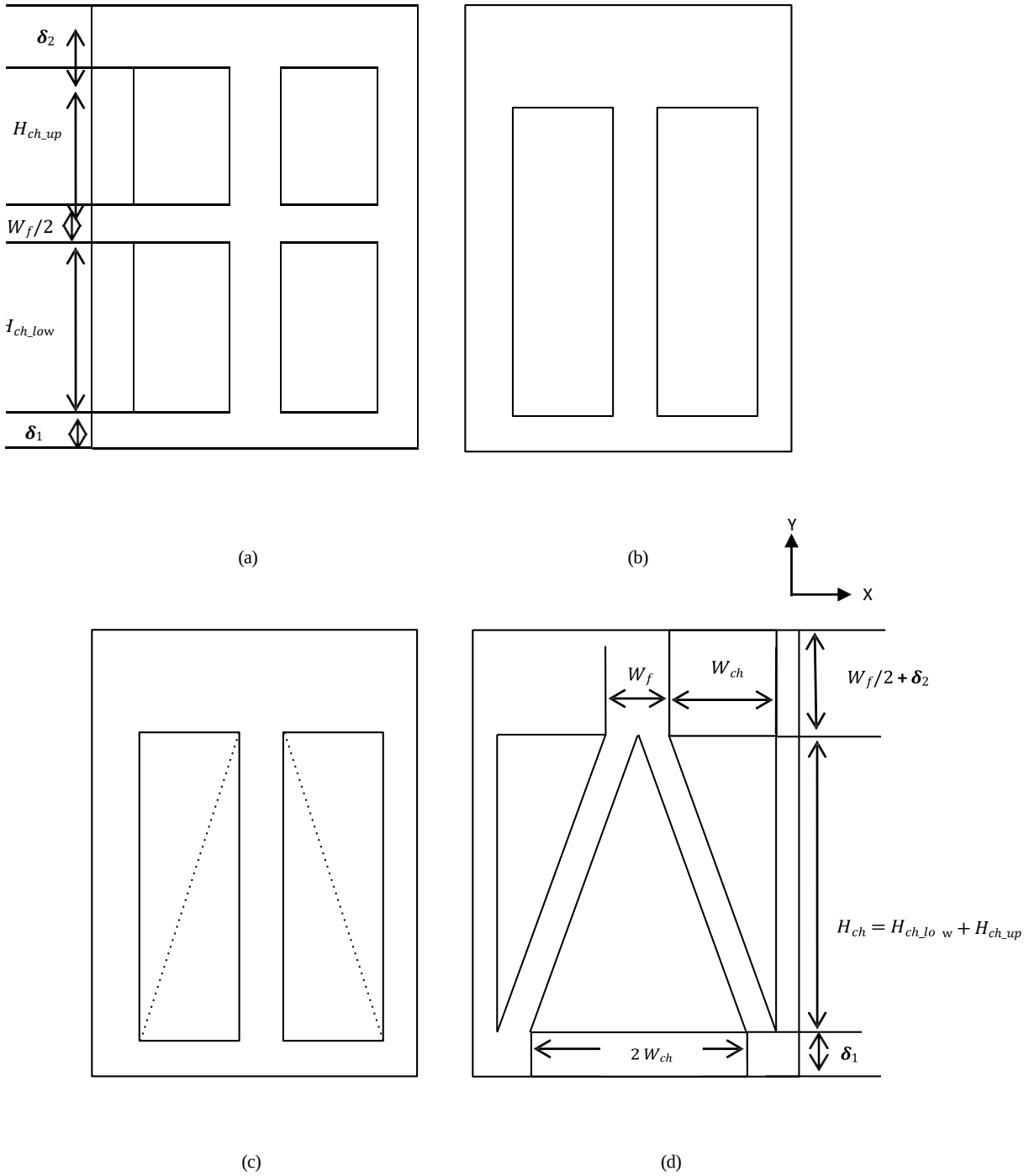

Fig. 1. (a) DL-MCHS (cross-sectional view) (b) Joining upper and lower layer. Two single layer channels are formed (c) intersecting channels diagonally (d) Microchannel sawtooth cooling device (cross-sectional view).

Mathematical modeling

Nanofluids are homogeneous mixtures of water and nanoparticles. Water is the base fluid in which nanoparticles are suspended. Steady-state governing equations for fluid flow and heat transfer are given below [15]. The continuity equation is the following:

$$\nabla.\vec{v} = 0 \quad (1)$$

Here, $\vec{v}$ is the mass average velocity.

The conservation of momentum equation is given below:

$$\nabla(\vec{v}.\vec{v}) = -\nabla P + \nabla\tau + \rho\vec{g} + \vec{F}_\sigma \quad (2)$$

In Eq. 2, ∇P is the pressure gradient, $\nabla\tau$ is the shear stress gradient, $\vec{g}$ is the gravitational acceleration, and $\vec{F}_\sigma$ is the surface tension force. For Newtonian fluids, the gradient of wall shear stress, $\nabla\tau = \mu_{eff}\nabla(\nabla\vec{v} + \vec{v}^T)$. Here, μ_{eff} is the effective dynamic viscosity of the nanofluid.

For the fluid domain, the conservation of energy equation is expressed as follows:

$$\nabla(T.\vec{v}) = \nabla(k_{eff}\nabla T) \quad (3)$$

In this equation, T is the temperature, and k_{eff} is the effective thermal conductivity of nanofluids.

For the solid domain, the energy balance equation is written as follows:

$$\nabla(k_s\nabla T_s) = 0 \quad (4)$$

Boundary Conditions

Boundary conditions in the computational domain are shown in Fig. 2.

Inlet: $T = T_{in}, \dot{m} = \dot{m}_{in}$

Outlet: $P = P_{out}$

Solid-fluid interface: A laminar sublayer is considered at the solid-fluid interface. Hence, heat is transferred from channel walls to the fluid by conduction. After achieving steady-state condition, fluid temperature at the laminar sublayer is the same as the adjacent wall temperature. Hence, the applied conditions are the following:

$$u = v = w = 0, T = T_s, |-k\nabla T|_n = |-k_s\nabla T_s|_n \quad (2)$$

Channel bottom wall: A uniform heat flux is applied at the bottom of the heat sink. Heat is transferred through the solid wall by conduction to the normal direction of the bottom surface. The heat transfer rate is calculated using the following equation:

$$q = -k_s\frac{\partial T_s}{\partial n} \quad (5)$$

Other channel walls: Other channel walls are considered insulated. Hence, heat loss from channel walls, $q_{loss} = 0$.

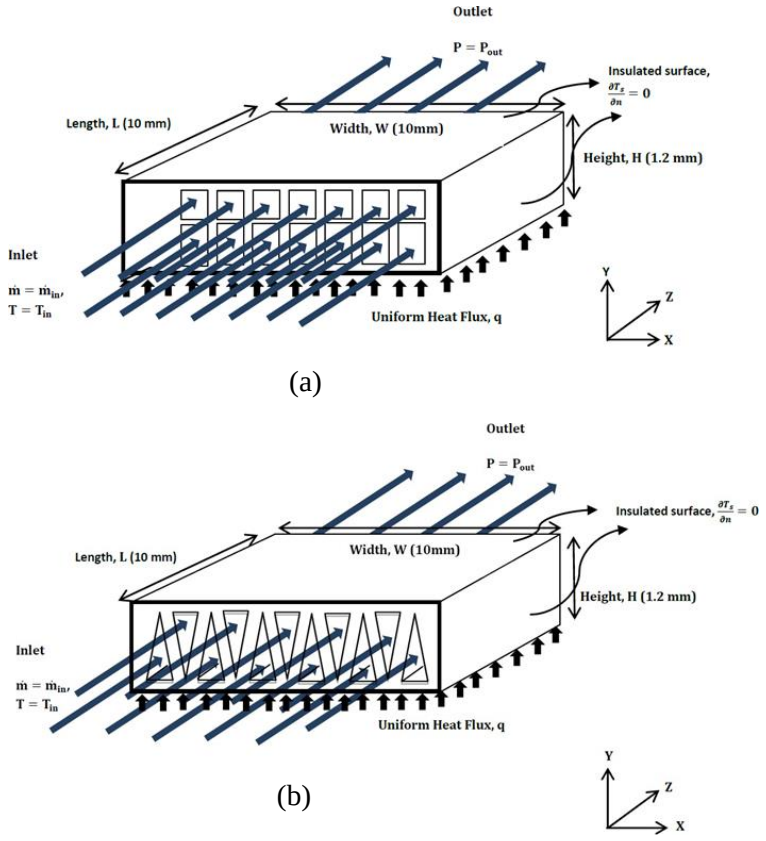

Fig. 2. Fluid flow and heat transfer in (a) double layer microchannel heat sink (b) microchannel sawtooth cooling device.

Effective Thermophysical Properties of Nanofluids

Effective dynamic viscosity is determined by the empirical correlation developed by Corcione 16, as given below:

$$\frac{\mu_{eff}}{\mu_f} = \frac{1}{1-34.87\left(\frac{d_p}{d_f}\right)-0.3\emptyset 1.03} \quad (6)$$

Here, μ_f is the dynamic viscosity of the base fluid, $\emptyset$ is the volume fraction of nano particles in the coolant, d_p is the particle diameter, and d_f is the equivalent molecular diameter of the base fluid. d_f is obtained from the following formula:

$$d_f = \frac{6M}{N\pi\rho_f} \quad (7)$$

In this equation, M represents the molecular weight of the base fluid, N is the Avogadro number, which is a constant and ρ_f is the density of the base fluid.

Table I. Thermophysical properties of materials at 298 K temperature

			Nano-particles		
Properties (unit)	Aluminum	Water	Al_2O_3	CuO	TiO_2
Density, $\rho(kg/m^3)$	2702	997	3970	6320	4157
Thermal conductivity,		0.607	36	76.5	8.4
$k(W/m.K)$		4180	765	6.27	710
Specific heat capacity,	273				
$c_p\ (J/kg.K)$					
	9030				
Dynamic viscosity, $\mu(Pa.s)$	–	890.3	–	–	–

Effective density is obtained from the following equation [16]:

$$\rho_{eff} = \alpha\rho_s + (1-\alpha)\rho_f \quad (8)$$

Specific heat capacity is calculated from the following correlation [16]:

$$c_{p,eff} = \frac{(1-\emptyset)(\rho_f c_{p,f})+\emptyset(\rho_p c_{p,p})}{(1-\emptyset)\rho_f+\emptyset\rho_p} \quad (9)$$

Effective thermal conductivity of the nanofluid is determined from the correlation developed by Chon et al. [17]. The correlation is given below:

$$\frac{k_{eff}}{k_f} = 1 + 64.7\emptyset^{0.7460}\left(\frac{d_f}{d_p}\right)^{0.3690}\left(\frac{k_p}{k_f}\right)^{0.7476} Pr^{0.9955}Re^{1.2321} \quad (10)$$

Various thermophysical properties of solid material, nanoparticles and base fluid measured at 293 K temperature are given in Table I.

Other equations

The convective heat transfer coefficient is calculated using the following formula:

$$h = \frac{q_{eff}N}{\sum_{n=1}^{N}(T_s-T_f)} \quad (11)$$

An equal number of nodes are considered on the solid and fluid domains to calculate the average temperature.

Effective heat flux: $q_{eff} = \dot{m}c_p(T_{out} - T_{in})$ (12)

Here $\dot{m}$ is the mass flow rate of the fluid. T_{out} and T_{in} are outlet and inlet temperatures, respectively.

Dimensionless numbers are calculated using the following formulas[18]

Nusselt number, $Nu = \frac{hD_h}{k_{eff}}$ (13)

Reynolds number, $Re = \frac{\rho_{eff}vD_h}{\mu_{eff}}$ (14)

D_h is the hydraulic diameter of the channel. Hydraulic diameters are calculated from the following formula[4]

Rectangular channel, $D_{h\_rec} = \frac{2ab}{a+b}$ (15)

Triangular channel, $D_{h\_tr} = \frac{4a}{P} = \frac{2ab}{a+\sqrt[2]{a^2+4b^2}}$ (16)

Total thermal resistance, the summation of conductive and convective thermal resistance, of the channel is considered to understand the heat transfer capability of the heat sink properly. It is written as follows:

$$R_{th} = R_{cond} + R_{conv} = \frac{H}{k_s A_s} + \frac{1}{hA_f} = \frac{T_{max}-T_{in}}{q_{eff}} \quad (17)$$

Here H is the total height of the heat sink, which is the heat conduction path in the solid domain. The area for heat conduction: $A_s = W_f \times L$ (18)

The contact area between solid and fluid:

$$A_f = \left[2W_{ch} + 4\left\{\sqrt{(H_{ch})^2 + \left(\frac{W_{ch}}{2}\right)^2}\right\}\right] \times L \quad (19)$$

Due to significant pressure drop, high pumping power is required to drive the fluid through microchannels. Pumping power: $\Omega = nvA_c\Delta P$ (20)

Here n is the number of channels, A_c represents the cross-sectional area of a single channel, and ΔP is the pressure drop inside the heat sink. Pressure drop is obtained by solving the conservation of momentum equation numerically.

Numerical simulation

Microchannel heat sinks have been simulated using commercial software FLUENT 14.5 release. Geometries were created by ANSYS Workbench Design Modeler. Heat sink and channel dimensions are provided in Table II.

Governing equations have been solved by the finite volume method. The second-order upwind scheme has been used for discretization. Semi-Implicit Method for Pressure Linked Equations (SIMPLE), developed by Patankar and Spalding 19, has been used to solve the pressure-velocity coupling equation. Residuals of solutions are monitored in FLUENT to ensure convergence.

Table II. Dimensions of heat sink and channels

Parameters (unit)	Value range
MCHS length, $L\ (mm)$	10
MCHS width, $W\ (mm)$	10
MCHS Height, $H\ (mm)$	1.2
Substrate thickness, $\delta_1 (mm)$	0.15
Width ratio, $\beta = \frac{W_f}{W_f+W_{ch}}$	0.4 - 1
Height ratio, $\gamma = \frac{H_{ch\_low}+H_{ch\_up}}{H}$	0.2 - 1

III. Results and Discussion

Effect of nano-particle volume fraction

According to Fig. 3, rectangular single-layer microchannel heat sinks have the highest overall thermal resistance, followed by rectangular double-layer and microchannel sawtooth cooling devices. Eq. 17 shows that system thermal resistance depends on conductive and convective thermal resistance. All channels have the same fin width and length (L), resulting in an identical area for heat conduction. Thus, only convection affects overall thermal resistance. Microchannel sawtooth cooling devices have more convection surface area than rectangular single- and double-layer channels. Because of this, its total thermal resistance is the lowest. DL-MCHS has lower thermal resistance than SL-channel. The thick wall between upper and lower channels acts as a fin in DL-MCHS. Convection occurs from the fin surface to the fluid. No fin separates upper and bottom layers in SL-MCHS. Hence, the convective heat transfer area is less than DL-MCHS.

Fig. 3 shows that total thermal resistance falls and then increases with nanoparticle volume fraction. Hung et al. [14] also noted this trend. As particle volume fraction increases, fluid thermal conductivity k_s increases. However, nanofluid dynamic viscosity falls, lowering the convective heat transfer coefficient h_f. Thus, convective thermal resistance rises and conductive thermal resistance decreases. First, conductive heat resistance decreases more than convective resistance. As a result total thermal resistance falls. Convective thermal resistance dominates heat sink thermal resistance for volume fractions over 2%. This increases total thermal resistance as the volume fraction of nanoparticles rise.

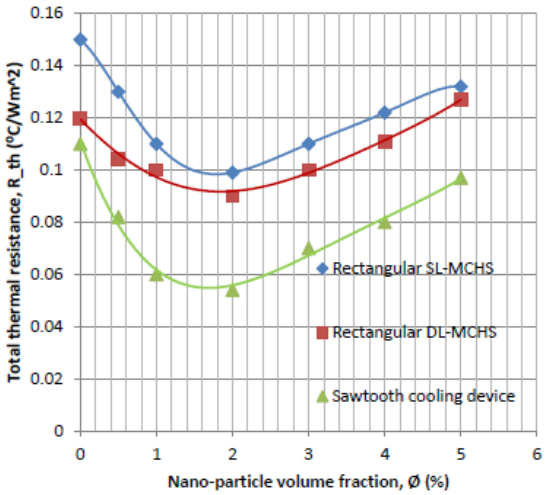

Fig. 3. Variation of total thermal resistance with volume fraction of nanoparticles for $\boldsymbol{\Omega} = 0.1$ W, $\beta = 0.6$, $\gamma = 0.2$ and $q = 1.81 \times 10^6$ Wm^{-2}.

Effect of channel dimensions

The channel width ratio (β) is calculated as $\beta = \frac{W_f}{W_f+W_{ch}}$. The convection area ($A_f$) decreases with the channel width (W_{ch}). Thus, convective thermal resistance rises. However, decreasing (W_{ch}) increases fin width (W_f). As the fin width rises, the area for heat conduction decreases conductive thermal resistance. As mentioned, conductive thermal resistance dominates, lowering overall thermal resistance. At β=0.65, convective thermal resistance dominates, and total thermal resistance rises with β. The curves are show in Fig. 4. Similar results were found by Hung et al.[14]

The channel height ratio, $\gamma = \frac{H_{ch\_low}+H_{ch\_up}}{H}$. As the height ratio increases, R_{th} increases and eventually drops (Fig. 5). By raising higher and lower channel heights, A_f rises. This lowers convective heat resistance (R_{conv}). Both fin thickness ($W_f/2$) and width (W_f) decrease. It reduces the conduction area (A_s). The conductive thermal resistance (R_{cond}) increases for this reason. Until γ=0.6, R_{cond} dominates over R_{conv}, leading to an increase in R_{th}. After reaching γ=0.4, R_{conv} dominates total thermal resistance. As the height ratio increases, R_{conv} drops.

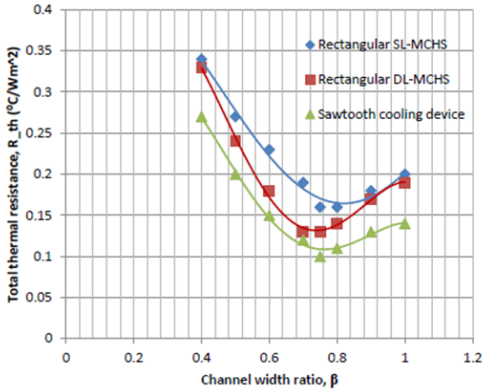

Fig. 4. Variation in total thermal resistance with channel width ratio for $\Omega = 0.1\,W$, $\emptyset = 0.02$, $\gamma = 0.2$ and $q = 1.81 \times 10^6\,Wm^{-2}$.

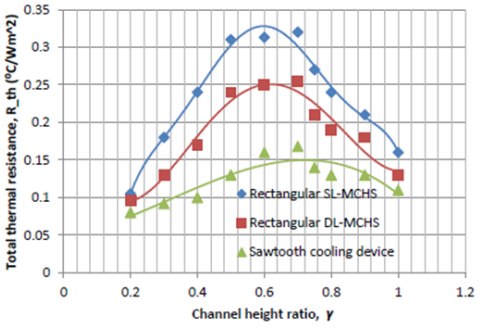

Fig. 5. Variation in total thermal resistance with channel height ratio for $\Omega = 0.1\,W$, $\emptyset = 0.02$, $\beta = 0.6$ and $q = 1.81 \times 10^6\,Wm^{-2}$.

Effect of pumping power

Fluid velocity at the inlet, $v_{in} = \frac{\dot{m}_{in}}{\rho A}$. Velocity as well as Reynolds number, Re increases with the increment of mass flow rate. As a result, convective heat transfer coefficient, h increases. Hence, in Fig. 6., Nusselt number augments with the increment of Reynolds number. However, it is observed that the curves are not linear. Increment of Nusselt number decreases for higher Reynolds numbers. Due to higher surface area, convective heat transfer in microchannel sawtooth cooling device is higher than rectangular single and double-layer channels. As a result, Nusselt number is also found higher in microchannel sawtooth cooling device than other two heat sinks.

As the increment of Nusselt number with Reynolds number is not consistent, decrement of total thermal resistance is also not steep for the total range of pumping power. In Fig. 7, total thermal resistance vs. pumping power has been plotted for three different types of nanofluids. It is observed that total thermal resistance first decreases steeply. However, slope of the curve decreases for higher pumping powers. Again, among three different nano-fluids, $Al_2O_3 +$ water, $CuO +$ water and $TiO_2 +$ water, $Al_2O_3 -$ water pair has shown the best performance.

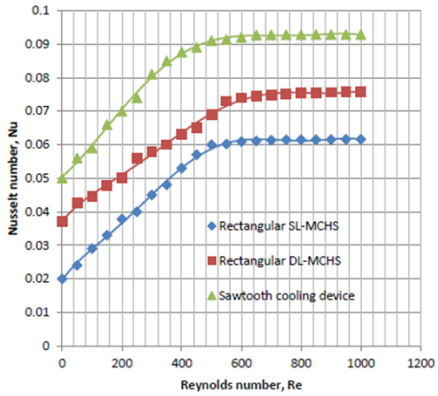

Fig. 6. Variation of Nusselt number with Reynolds number for $\emptyset = 0.02$, $\beta = 0.6$, $\gamma = 0.2$ and $q = 1.81 \times 10^6\,Wm^{-2}$.

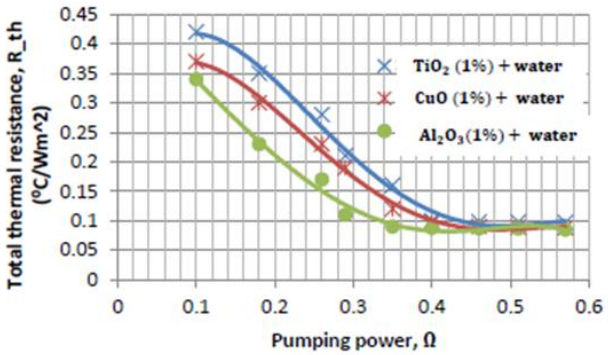

Fig. 7. Total thermal resistance vs. pumping power for $\emptyset = 0.02$, $\beta = 0.6$, $\gamma = 0.2$ and $q = 1.81 \times 10^6\,Wm^{-2}$.

IV. Conclusion

Double-layer microchannel heat sink has been modified to form single-layer microchannel heat sink and microchannel sawtooth cooling device. Numerical analysis of heat transfer and pressure drop in these heat sinks for three distinguished nano-fluids has been carried out. Comparisons have been made between these heat sinks. In a nutshell, findings are following:

i. Order of total thermal resistance from higher to lower: SL-MCHS > DL-MCHS > microchannel sawtooth cooling device.

ii. Total thermal resistance first decreases and then increases with the increment of volume fraction of nanoparticles and channel width ratio. On the other hand, total thermal resistance first augments and then decreases with the increment of channel height ratio. These affects are originated from the dominance of conductive or convective thermal resistance on total thermal resistance.

iii. Total thermal resistance does not decrease sharply for total range of pumping power. Hence, increment of pumping power is not always cost effective.

iv. Heat transfer rate from higher to lower order among three different nano-fluids used: $Al_2O_3 +$ water > $CuO +$ water > $TiO_2 +$ water.

References

1. Tuckerman, David B., and Roger Fabian W. Pease, 1981. High-performance heat sinking for VLSI. IEEE Electron device letters 2, no. 5, 126-129. https://ieeexplore.ieee.org/abstract/document/1481851

2. Dickey J. T. and T. T. Lam, 2006. U.S. Patent No. 6,983,792. Washington, DC: U.S. Patent and Trademark Office.

3. Gunnasegaran, Prem, H. A. Mohammed, N. H. Shuaib, and Rahman Saidur, 2010. The effect of geometrical parameters on heat transfer characteristics of microchannels heat sink with different shapes. International communications in heat and mass transfer 37, no. 8, 1078-1086. https://downloads.hindawi.com/archive/2012/832708.pdf

4. Asgari, Omid, and Mohammad Hassan Saidi, 2009. Approximate method of determining the optimum cross section of microchannel heat sink. Journal of mechanical science and technology 23, 3448-3458. https://link.springer.com/article/10.1007/s12206-009-1018-8

5. Xia, Guodong, Lei Chai, Haiyan Wang, Mingzheng Zhou, and Zhenzhen Cui, 2011. Optimum thermal design of microchannel heat sink with triangular reentrant cavities. Applied Thermal Engineering **31, (6-7).** 1208-1219. https://www.sciencedirect.com/science/article/abs/pii/S1359431110005387

6. Kim, Sung-Min, and Issam Mudawar, 2010. Analytical heat diffusion models for different micro-channel heat sink cross-sectional geometries. International Journal of Heat and Mass Transfer 53, no. 19-20. 4002-4016. https://www.sciencedirect.com/science/article/abs/pii/S0017931010002619

7. Vafai, Kambiz, and Lu Zhu. Analysis of two-layered micro-channel heat sink concept in electronic cooling, 1999. International Journal of Heat and Mass Transfer **42, (12).** 2287-2297. https://www.sciencedirect.com/science/article/abs/pii/S0017931098000179

8. Manaf, Hazli, Shugata Ahmed, Mirghani I. Ahmed, and M. N. A. Hawlader, 2015. A triangular double layer microchannel heat sink: effect of parallel and counter flow. Advanced Materials Research 1115. 433-439. https://www.scientific.net/AMR.1115.433

9. Seder, I. M., M. I. Ahmed, S. Ahmed, and M. N. A. Hawlader, 2014. Feasibility of double-layer microchannel fabrication at low speed micro end-mill and wire-cut EDM machines. Australian Journal of Basic and Applied Sciences **8, (15)**, 211-217.

10. Hung, Tu-Chieh, and Wei-Mon Yan, 2012. Enhancement of thermal performance in double-layered microchannel heat sink with nanofluids. International Journal of Heat and Mass Transfer **55, (11)**-12, 3225-3238. https://www.sciencedirect.com/science/article/abs/pii/S0017931012001202

11. Wong, Kok-Cheong, and Fashli Nazhirin Ahmad Muezzin, 2013. Heat transfer of a parallel flow two-layered microchannel heat sink. International communications in heat and mass transfer 49, 136-140. https://www.sciencedirect.com/science/article/abs/pii/S0735193313001899

12. Chong, S. H., K. T. Ooi, and T. N. Wong, 2002. Optimisation of single and double layer counter flow microchannel heat sinks. Applied Thermal Engineering **22,(14),** 1569-1585. https://www.sciencedirect.com/science/article/abs/pii/S1359431102000832

13. Shao, Baodong, Lifeng Wang, Heming Cheng, and Jianyun Li, 2012. Optimization and numerical simulation of multi-layer microchannel heat sink. Procedia Engineering **31,** 928-933. https://www.sciencedirect.com/science/article/pii/S1877705812011472

14. Hung, Tu-Chieh, Wei-Mon Yan, and Wei-Ping Li, 2012. Analysis of heat transfer characteristics of double-layered microchannel heat sink. International Journal of Heat and Mass Transfer 55, no. 11-12, 3090-3099. https://www.sciencedirect.com/science/article/abs/pii/S0017931012001019

15. H. L. John, 2011. A heat transfer textbook. Phlogiston press, Massachusetts, USA.

16. Corcione, Massimo, 2010. Heat transfer features of buoyancy-driven nanofluids inside rectangular enclosures differentially heated at the sidewalls. International Journal of Thermal Sciences 49, no. 9. 1536-1546. https://www.sciencedirect.com/science/article/abs/pii/S129007291000133X

17. Chon, Chan Hee, Kenneth D. Kihm, Shin Pyo Lee, and Stephen US Choi. 2005. Empirical correlation finding the role of temperature and particle size for nanofluid (Al_2O_3) thermal conductivity enhancement. Applied Physics Letters 87, no. 15. https://pubs.aip.org/aip/apl/article-abstract/87/15/153107/328217/Empirical-correlation-finding-the-role of?redirectedFrom=fulltext

18. Bergman, Theodore L, 2011. Fundamentals of heat and mass transfer. John Wiley & Sons.

19. Patankar, Suhas V., and D. Brian Spalding. 1983. A calculation procedure for heat, mass and momentum transfer in three-dimensional parabolic flows. Numerical prediction of flow, heat transfer, turbulence and combustion, pp. 54-73. https://www.sciencedirect.com/science/article/abs/pii/B9780080309378500131